Applied Catalysis B: Environmental 111–112 (2012) 334–341

Contents lists available at SciVerse ScienceDirect

Applied Catalysis B: Environmental

journal homepage: www.elsevier.com/locate/apcatb

Solvothermal synthesis of flower-like BiOBr microspheres with highly visible-light photocatalytic performances

Yuning Huo*, Jia Zhang, Miao Miao, Yi Jin

The Education Ministry Key Lab of Resource Chemistry, Shanghai Key Laboratory of Rare Earth Functional Materials, Shanghai Normal University, Shanghai 200234, China

ARTICLE INFO

Article history:
Received 11 June 2011
Received in revised form 9 October 2011
Accepted 10 October 2011
Available online 17 October 2011

Keywords:
Hierarchical flower-like BiOBr microsphere
Solvothermal preparation
Two-component solvent
Visible-light photocatalyst
Degradation of rhodamine B

ABSTRACT

Hierarchical flower-like BiOBr microspheres assembled with nanosheets were synthesized via solvothermal method with both two-component solvent (ethylene glycol and isopropanol) and CTAB surfactant. The growth of BiOBr crystal was significantly influenced by the concentration of ethylene glycol and isopropanol in two-component solvent, the amount of CTAB surfactant and the solvothermal time. According to the photodegradation of rhodamine B (RhB) under visible-light irradiations, the high photocatalytic activity of hierarchical flower-like BiOBr microspheres could be ascribed to the enhanced visible-light absorbance via the light multi-reflections, the efficient separation of photo-generated electrons and holes, the high crystallization and the large surface area. The main active species during the photocatalytic reaction was determined as $^{\bullet}O_2^-$ radical by additionally dissolving the trapping agent in the solution. Meanwhile, BiOBr microspheres also exhibited the excellent durability owing to the stable crystal phase and microsphere morphology.

1. Introduction

Semiconductor photocatalysts have caused significant attentions because of their applications in decomposing organic compounds and water splitting [1,2]. TiO_2 photocatalyst has been mostly developed owing to its advantages of cheapness, nontoxicity and stability [3,4]. However, the practical application of TiO_2 is still limited due to no light absorption within the visible-light region and the low quantum efficiency. Therefore, great efforts have been made to achieve the modified TiO_2 [5–7] and novel non-TiO_2 semiconductors [8–10]. In recent years, bismuth-based oxyhalides, BiOX (X=Cl, Br or I), have been attracted many attentions owing to its potential photocatalysis application [11–13], besides being applied in ionic conduction, ferroelectric materials and pigments [14,15]. Among these BiOX catalysts, BiOBr is an active and stable photocatalyst under visible-light irradiations, which has layered tetragonal matlockite structure with $[Bi_2O_2]$ slabs interleaved by double slabs of halogen atoms [16,17].

To date, various synthesis methods have been developed successfully to prepare BiOBr particles, such as hydrolysis process [18,19], reverse micro-emulsion synthesis [20] and solvothermal process [11,21]. The obtained BiOBr catalyst presents different morphologies including nano-scale particle, nanosheet and micro-scale morphology assembled with nanosheet. As we known, the micrometer 3D architecture with nano-scale building blocks is effective during the photocatalysis application, considering the enhanced light-harvesting capacity, the prevention of aggregation and the easy solid/liquid separation [17,22,23]. However, how to obtain the desired micrometer architectures of BiOBr catalyst to achieve the efficient visible-light harvesting and the high photoactivity is still in need of further exploration.

Herein, we report a novel preparation approach of hierarchical flower-like BiOBr microspheres via the solvothermal method in two-component solvent, assisted with surfactant acted as both Br source and template simultaneously. The growth of BiOBr crystal has been investigated by adjusting various synthesis conditions. The high visible-light photocatalytic activity for RhB degradation on flower-like BiOBr microspheres is closely related to the enhanced light absorbance owing to the light multi-reflections. The active species during the photodegradation reaction are determined. Furthermore, the BiOBr catalyst also can be easily recycled and repetitively used for many times.

2. Experimental

2.1. Catalyst preparation

All the chemicals were of analytic purity and used without further purification. In a typical process, 0.12 g $Bi(NO_3)_3{\cdot}5H_2O$ was dissolved into 40.0 mL solution mixed with both ethylene glycol and isopropanol. Then, the cetyltrimethylammonium bromide (CTAB) with desired amount was added into the solution and

* Corresponding author. Tel.: +86 21 6432 2272; fax: +86 21 6432 2272.
E-mail address: huoyuning@shnu.edu.cn (Y. Huo).

0926-3373/$ – see front matter © 2011 Elsevier B.V. All rights reserved.
doi:10.1016/j.apcatb.2011.10.016

stirred at 30 °C until a transparent solution was obtained. Subsequently, the solution was transferred into a 50 mL Teflon-lined stainless steel autoclave with 80% volume filled. The autoclave was sealed and maintained at 160 °C for various time interval followed by naturally cooling to room temperature. The obtained yellow powder was filtered and washed with deionized water for more than 3 times and dried at 80 °C for 12 h. Finally, the powder was calcined at 400 °C for 4 h to improve the crystallization of sample and remove the organic residuals. The as-prepared samples were denoted as BOB–*X*–*Y*–*Z*, where *X*, *Y* and *Z* represented the ethylene glycol amount (mL), Br/Bi molar ratio and solvothermal time (h), respectively. For comparison, the sample with the substitution of ethylene glycol with glycerol was referred to BOB–5–2–12(GLY). BOB–5–2–12(ETH) and BOB–5–2–12(TBA) expressed the substitution of isopropanol with ethanol and tert-butyl alcohol, respectively. BOB–5–2–12(G) was obtained by crushing BOB–5–2–12 sample and BOB–Ref was prepared according to the previous report [24].

2.2. Characterization

The sample composition was determined by energy dispersive X-ray spectroscopy (EDX, JEM-2100). The structure was examined by X-ray diffraction (XRD, Rigacu D/Max-2000) and selected area electronic diffractions (SAED, JEM-2010). The crystallite size was calculated based on the Scherrer equation ($D = K\lambda/\beta\cos\theta$). Surface morphologies were observed by scanning electron microscopy (FESEM, HITACHI S-4800) and transmission electronic microscopy (TEM, JEM-2010). X-ray photoelectron spectroscopy (XPS, Versa Probe PHI 5000) was employed to determine surface electronic states. The shift of the binding energy due to relative surface charging was corrected using the C_{1S} level at 284.8 eV as an internal standard. N_2 adsorption–desorption isotherms were measured on a Quantachrome NOVA 4000e at 77 K. The Brunauer–Emmett–Teller (BET) method was used to calculate the specific surface area (S_{BET}) based on the adsorption branches. The thermal stability was investigated by a thermogravimetric analyzer (DTG-60H). The optical property was analyzed by both UV–vis diffuse reflectance spectra (DRS, MC-2530) and photoluminescence spectra (PLS, Varian Cary-Eclipse 500). The electron spin resonance (ESR) spectra were detected on a Bruker model A300 spectrometer under visible light irradiation ($\lambda > 420$ nm) with the settings of center field (3512.48 G), microwave frequency (9.86 GHz) and power (6.35 mW). The radical capture agent was 5,5-dimethyl-L-pyrroline-N-oxide (DMPO) dissolved in distilled water (for $^{\bullet}OH$) or methanol (for $^{\bullet}O_2$), respectively.

2.3. Photocatalytic test

Liquid-phase photocatalytic degradation of rhodamine B (RhB) was carried out at 30 °C in an 80 mL self-designed quartz photochemical reactor containing 25.0 mg catalyst and 50.0 mL 20.0 mg/L RhB aqueous solution. The reaction system was stirred vigorously (>800 rpm) to eliminate diffusion effect on the reaction kinetics. After reaching adsorption equilibrium for 1 h, the photocatalytic reaction was initiated by irradiating the system with one 500 W xenon lamp (CHF-XM500, light intensity = 600 mW/cm^2) located at 18 cm away from the reaction solution. To make sure that the photocatalytic reaction was really driven by visible-light, all the UV lights with the wavelength less than 420 nm were removed by a glass filter (JB-420). At given time intervals, the concentration of RhB left in the solution was determined by the UV–vis spectroscopy (UV-7504/PC) at its characteristic wavelength of 553 nm. After the reaction, little organic byproducts could be identified by HPLC–MS in the solution. Preliminary tests demonstrated a good linear relationship between the light absorbance and RhB concentration.

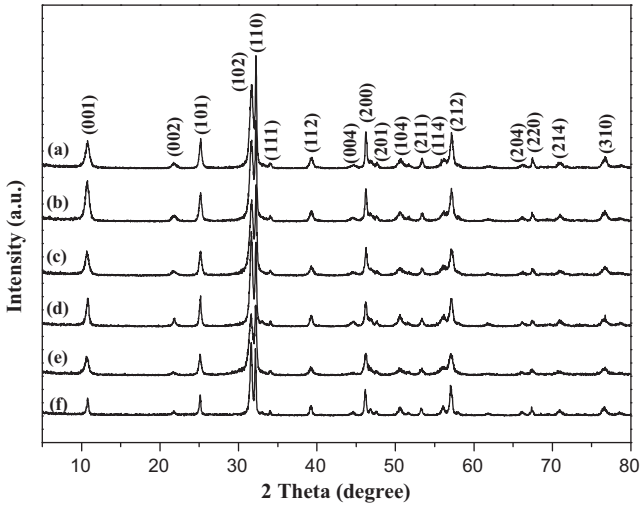

Fig. 1. XRD patterns of (a) BOB–2–2–12, (b) BOB–5–2–12, (c) BOB–10–2–12, (d) BOB–20–2–12, (e) BOB–30–2–12 and (f) BOB–40–2–12 samples.

Meanwhile, experimental results also confirmed that only less than 6.0% RhB was adsorbed by catalysts after reaction without light irradiation, and only 4.0% RhB was decomposed under light irradiation in the absence of catalysts, and thus could be neglected in comparison with the photocatalysis process. The reproducibility of the results was checked by repeating the experiments at least three times and was found to be within acceptable limits (±5%). The active species during the photocatalytic reaction were determined by additionally dissolving 0.050 mmol trapping agents including EDTA, $AgNO_3$, tert-butyl alcohol (TBA) and benzoquinone (BQ), which could capture photo-generated holes, photo-generated electrons, $^{\bullet}OH$ radical and $^{\bullet}O_2^-$ radical, respectively [25–27]. After the reaction, the trapping agents were still existed in the solution. The durability of catalyst was measured according to the following procedure. After each run of photocatalysis reactions, the photocatalyst was separated from aqueous solution by centrifugation, washed with distilled water for 3 times and dried at 100 °C for 12 h. Then, each recycling test was conducted under the same conditions for 50 min and the RhB photodegradation rate was determined to show the change of activity.

3. Results and discussion

3.1. Characterization of BiOBr catalysts

3.1.1. XRD and EDX patterns

XRD patterns in Fig. 1 demonstrated that all of BOB–*X*–2–12 samples were in pure BiOBr crystal phase with high crystallization. All the detectable peaks could be assigned to the tetragonal BiOBr (JCPDS 09-0393) [24] and no other diffraction peaks could be found. Meanwhile, the crystallite sizes based on the principal (1 1 0) diffraction peak were summarized in Table 1. BOB–40–2–12 revealed the larger crystallite size than other BOB–*X*–2–12 samples with similar size, implying the inhibition effect of isopropanol to the growth of BiOBr crystal. Based on the EDX pattern in Fig. S1, the molar ratio of Bi:O:Br in BOB–5–2–12 was approximately equal to 1:1:1, also confirming the formation of BiOBr.

3.1.2. XPS spectra

XPS spectra (Fig. 2) for the measurement of surface compositions and chemical states also showed that pure BiOBr catalyst was formed without either Bi_2O_3 [28] or metallic Bi [29] species. Two peaks at 159.2 and 164.5 eV were attributed to $Bi_{4f7/2}$ and $Bi_{4f5/2}$, respectively, indicative of Bi^{3+} in BiOBr. The $Br_{3d5/2}$ and $Br_{3d3/2}$

Table 1
Structure parameters and photoactivities of different samples.

Sample	Crystallite size (nm)	S_{BET} (m^2/g)	Photodegradation rate (%)	k (min^{-1})
BOB–2–2–12	27.5	21.5	90	0.0675
BOB–5–2–12	27.6	23.7	95	0.0771
BOB–10–2–12	26.8	18.3	41	0.0236
BOB–20–2–12	26.4	16.2	35	0.0169
BOB–30–2–12	28.1	15.1	34	0.0156
BOB–40–2–12	35.7	13.9	18	0.00376
BOB–5–2–12(G)	/	24.2	57	0.0336
BOB–Ref	39.8	17.0	51	0.0310

Reaction conditions: 25.0 mg catalyst, 50.0 mL 20.0 mg/L RhB aqueous solution, reaction temperature = 30 °C, one 500 W Xe lamp (light intensity = 600 mW/cm^2, $\lambda > 420$ nm), reaction time = 40 min.

peaks were associated with the binding energy at 68.4 and 69.2 eV, respectively. The O_{1S} peak could be fitted by two peaks at 530.1 and 531.7 eV (dash lines), which were related to the oxygen in BiOBr catalyst and other components (such as –OH and H_2O) adsorbed on the surface of BiOBr, respectively [11,30].

3.1.3. TG–DTA patterns

TG–DTA patterns in Fig. S2 presented that no significant weight loss and exothermic peak were existed in BOB–5–2–12 sample when the temperature was lower than 610 °C, indicative of the thermal stability of catalyst and the complete removal of organic residues after calcination. The weight loss at higher temperature was owing to the decomposition of BiOBr with the exothermic peak at 714 °C.

3.1.4. FESEM and TEM images

From FESEM images in Fig. 3, all of BOB–*X*–2–12 samples exhibited the hierarchical flower-like microspheres assembled by nanosheets with a high yield since no other morphologies were observed. With the increased concentration of ethylene glycol, the diameter of microspheres varied from about 1.0 to 5.0 μm with gradually aggregated nanosheets and the thickness of nanosheets increased from about 5 to 10 nm, according to the high-resolution FESEM images (not shown). The TEM image of BOB–5–2–12 in Fig. 4 also showed the flower-like BiOBr microsphere with the solid interior was assembled by nanosheets. Moreover, HRTEM image confirmed the high crystallization of BiOBr catalyst, corresponding to the ordered lattice fringes with an inter-planar space of 0.278 nm for (1 1 0) plane. The SAED pattern of an individual nanosheet presented the well-defined electron diffraction spot, which demonstrated the single crystal nature of nanosheet. The bright spots could be indexed to (1 1 0) and (1 0 0) plane of tetragonal BiOBr crystal, respectively. Meanwhile, the lattice parameters (a = 8.484 Å and c = 5.813 Å) presented no change in different samples according to XRD results, implying that adjusting the reactants and solvents could only influence the aggregation of crystal grains and thus obtain the different crystallite size, but could not affect the crystal lattice.

3.1.5. N_2 adsorption–desorption isotherms

The S_{BET} and porosity of BOB–5–2–12 were investigated via N_2 adsorption–desorption isotherms, as shown in Fig. S3. The isotherm could be categorized as type IV with the distinct hysteresis loop at about p/p_o = 0.5–1.0, indicative of the mesoporous structure. The inserted pore diameter distribution mainly revealed the mesoporous diameter of about 4.0 nm, which could be considered as the result of the self-assembly of CTAB surfactant. Additionally, the S_{BET} of BOB–*X*–2–12 samples summarized in Table 1 exhibited the decreased trend with the increased amount of ethylene glycol, owing to the enhanced particle size and the aggregation of nanosheets.

3.1.6. Plausible mechanism of BiOBr formation

In order to investigate the plausible formation mechanism of hierarchical BiOBr microspheres, the influence of both solvothermal time and reactants were also analyzed via comparing different samples with XRD patterns and FESEM images. From XRD patterns in Fig. S4, BOB–5–2–*Z* samples displayed the improved crystallization of pure BiOBr crystal with the increase of solvothermal time. The crystallite size was enhanced gradually before 12 h and remained within the further increased time, in accordance with the crystal growth process presented in FESEM images (Fig. S5). At the initial time of 0.5 h, small nanosheets in irregular shape were formed with the in-plane size of about 100–300 nm and thickness of about 20 nm. Then, the nanosheets exhibited the gradual agglomeration after 1 h and oriented attachment at 2 h to form the initial flower-like morphology. At the solvothermal time of 6 h, the integrate flower-like microspheres were formed with larger and thinner nanosheets (about 10 nm thickness). Further increasing the solvothermal time

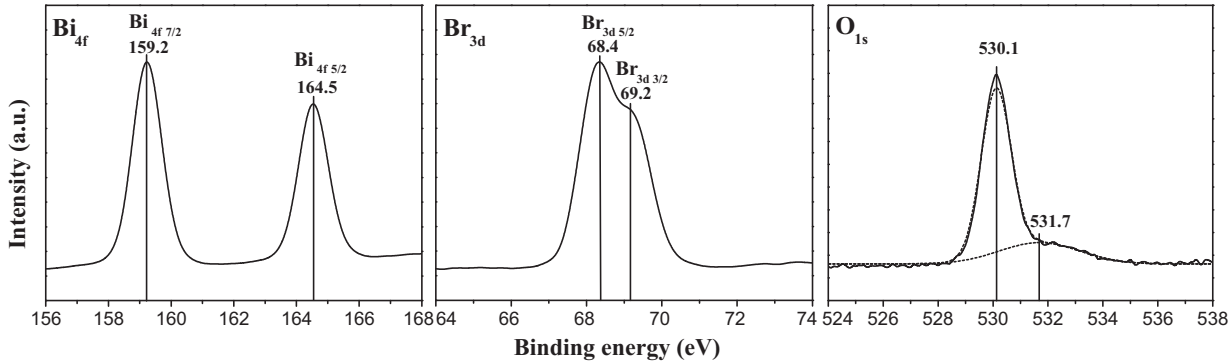

Fig. 2. XPS spectra of BOB–5–2–12 sample.

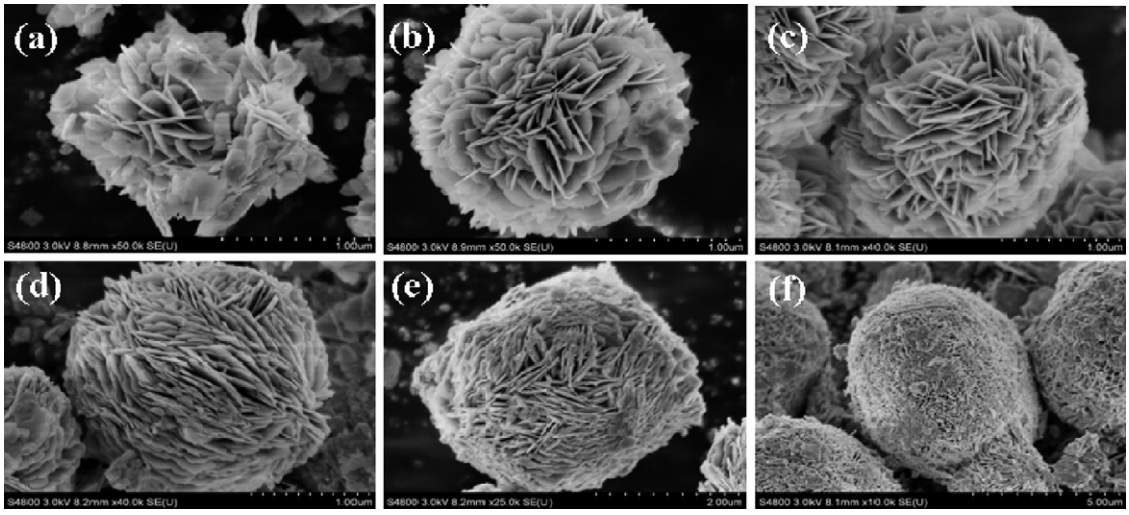

Fig. 3. FESEM morphologies of (a) BOB–2–2–12, (b) BOB–5–2–12, (c) BOB–10–2–12, (d) BOB–20–2–12, (e) BOB–30–2–12 and (f) BOB–40–2–12 samples.

to 12 h could achieve the larger microspheres, in which the diameter was about 1.5 μm and the nanosheet thickness was less than 10 nm. The same morphology was reserved until the solvothermal time of 24 h, corresponding to the similar crystallite size. Meanwhile, the increased molar ratio of Br/Bi could also enhance the crystallization of BiOBr catalyst, according to XRD patterns of BOB–5–Y–12 samples in Fig. S6. The crystallite size was increased from 13.7 nm in BOB–5–1–12 to 28.2 nm in BOB–5–4–12, corresponding to FESEM images in Fig. S7. The diameter of BiOBr microspheres was greatly improved from about 1.5 to 6.0 μm and the thickness of nanosheets was decreased from >15 nm to <10 nm, indicative of the significant role of surfactant to crystal growth. When glycerol acted as the solvent instead of ethylene glycol in BOB–5–2–12(GLY), the crystallization of BiOBr catalyst was significantly inhibited (see XRD patterns in Fig. S8) with much smaller crystallite size (11.2 nm), comparing to that of BOB–5–2–12. However, the substitution of isopropanol with ethanol in BOB–5–2–12(ETH) or tert-butyl alcohol in BOB–5–2–12(TBA) led to the similar crystallization and the crystallite size (26.6 and 27.7 nm, respectively) as that of BOB–5–2–12, as shown in Fig. S9. Meanwhile, FESEM images in Fig. S10 revealed larger microspheres (about 4.5 μm diameter) with smaller nanosheets in BOB–5–2–12(GLY) than that in BOB–5–2–12 and the morphology in both BOB–5–2–12(ETH) and BOB–5–2–12(TBA) was similar to that in BOB–5–2–12, in accordance with the XRD results.

Based on the above discussion, the plausible mechanism of BiOBr crystal growth could be proposed according to Scheme 1. The coordination of ethylene glycol with Bi^{3+} could result in the formation of alkoxides ($Bi(OCH_2CH_2OH)^{2+}$), which was stable as a dense and linearly aligned structure [31,32]. However, the substitution of ethylene glycol by glycerol was unfavorable to the coordination with Bi^{3+} and the further crystallization of BiOBr nanosheets, possibly owing to the sterically hindering effect of glycerol. Meanwhile, CTAB surfactant which acted as both template and Br source was self-assembled to form the lamellar structure [24]. Subsequently, the combination of Br^- in CTAB lamellas with $Bi(OCH_2CH_2OH)^{2+}$ induced the formation of BiOBr nanosheets during the solvothermal process. The higher concentration of CTAB surfactant could lead to the thinner nanosheets, indicative of the significant effect of CTAB micelle to the anisotropical growth of BiOBr crystals [33]. Isopropanol in the two-component solvent also presented the distinct influence during the formation of nanosheets. The high concentration of isopropanol between nanosheets could significantly inhibit the agglomeration of nanosheets and the corresponding low concentration of ethylene glycol was not beneficial to the coordination

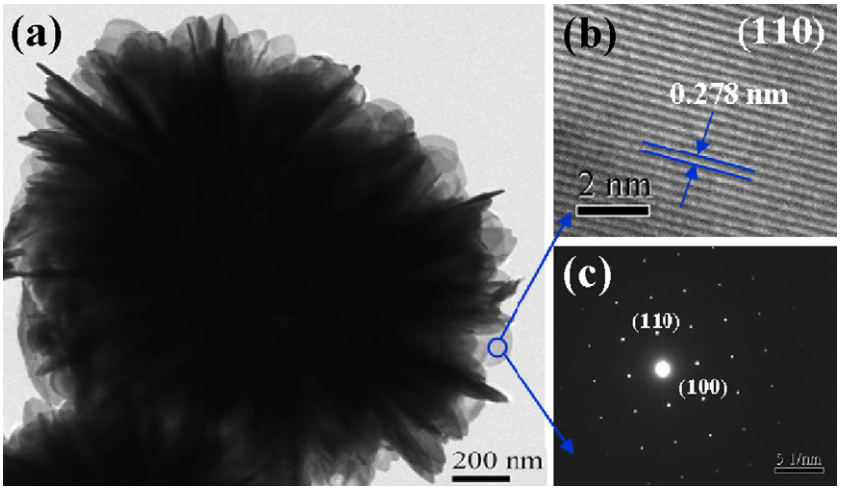

Fig. 4. (a) TEM, (b) HRTEM and (c) SAED images of BOB–5–2–12 sample.

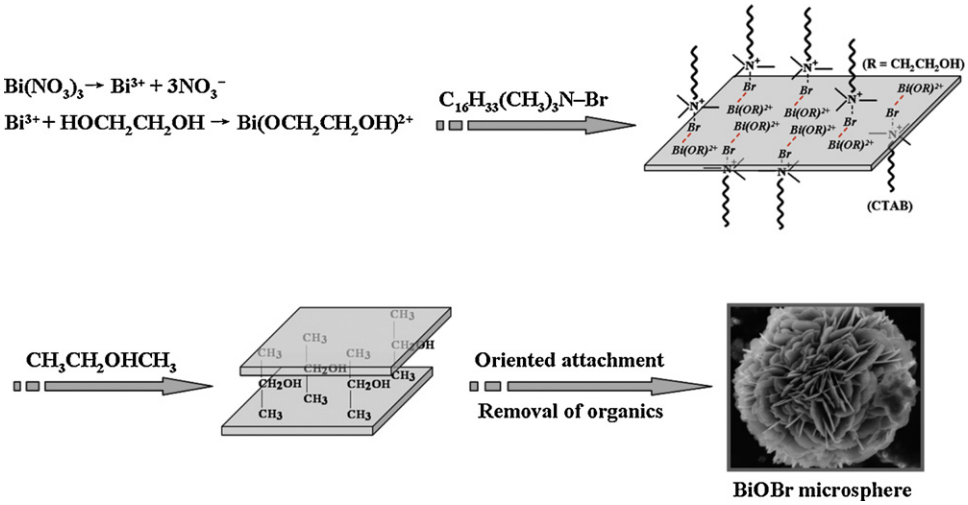

Scheme 1. The plausible formation mechanism of flower-like BiOBr microsphere.

with Bi^{3+}, leading to the small hierarchical flower-like microspheres. Both ethanol and tert-butyl alcohol played the same role as isopropanol during the BiOBr crystal growth, due to the similar molecular size as that of isopropanol. Finally, in order to minimize the surface energy, BiOBr nanosheets were agglomerated via oriented attachment and the stable flower-like BiOBr microspheres were created after the removal of organics via calcination. To sum up, both solvent and surfactant could affect the crystallite size and the growth trend significantly. Ethylene glycol played the key role to coordinate with Bi^{3+}, glycerol was not benefit to the coordination with Bi^{3+} and lead to the smaller crystallite size of BiOBr, isopropanol could also decrease the crystallite size and mainly inhibit the agglomeration of nanosheets, and ethanol or tert-butyl alcohol behaved the similar influence as isopropanol to the crystallite size and microsphere size. Additionally, the increased concentration of CTAB surfactant promoted the crystallite size of BiOBr with larger microsphere size and thinner nanosheets.

3.2. Optical property

The optical properties of BiOBr samples were measured by UV–vis DRS and PL spectra. From UV–vis DRS spectra in Fig. 5, BiOBr samples revealed much stronger absorption in visible-light region than P25 TiO_2. According to following formula [34]:

$$(\alpha h\upsilon)^n = k(h\upsilon - E_g)$$

where α, υ, k, and E_g were the absorption coefficient, light frequency, proportionality constant and band gap, respectively. We plotted $(\alpha h\upsilon)^{1/2}$ *vs* $h\upsilon$ (see the insert in Fig. 5). From the extrapolated intercept, the E_g of BOB–5–2–12 was determined as 2.9 eV, lower than that of P25 TiO_2, in accordance with the previous reports [19]. Furthermore, both BOB–5–2–12 and BOB–40–2–12 showed higher visible-light absorption than BOB–5–2–12(G), which was BOB–5–2–12 sample after being crushed (see FESEM image in Fig. S11), implying that more light reflection could be achieved within flower-like microspheres assembled with nanosheets. The light absorbance of BOB–5–2–12 was stronger than that of BOB–40–2–12, since the space between nanosheets in BOB–5–2–12 was favorable for the entry of visible light and the light multi-reflections [35] could be enhanced within the flower-like microspheres.

The recombination of photo-induced electrons and holes in the semiconductor could be verified by PL spectra. According to Fig. 6, BOB–5–2–12 exhibited weaker intensity of peak at 560 nm than both BOB–40–2–12 and BOB–Ref, corresponding to the

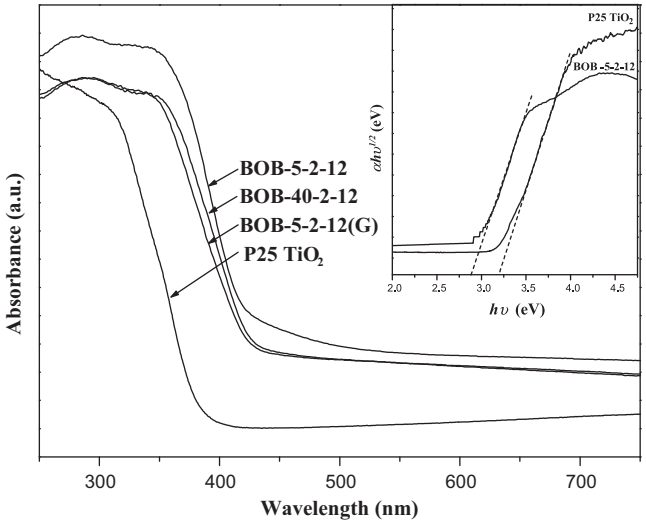

Fig. 5. UV–vis diffuse reflection spectra of different catalysts. The inset shows the optical absorption edges.

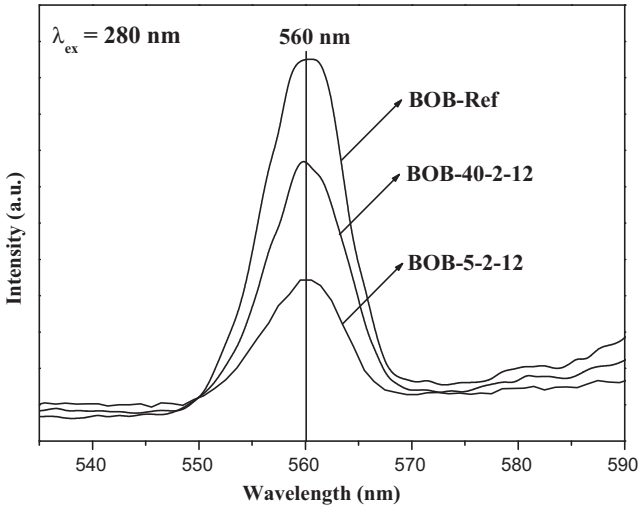

Fig. 6. PL spectra of different samples with the excitation wavelength of 280 nm.

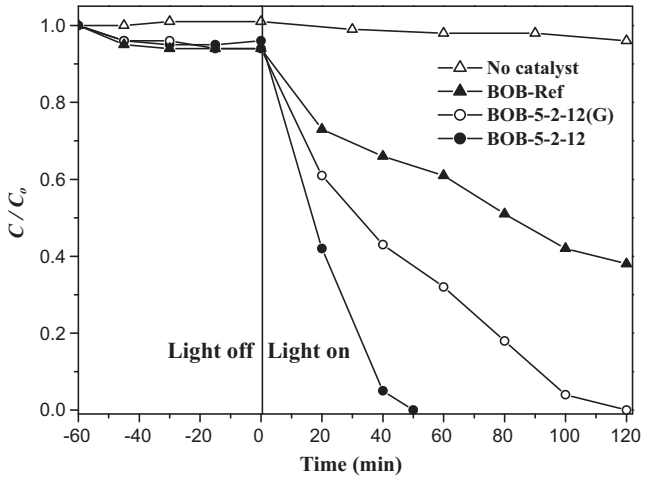

Fig. 7. Reaction process for photocatalytic degradation of RhB with different catalysts and without catalyst. C_0 and C referred to the initial RhB concentration and the RhB concentration determined at different reaction time, respectively. Reaction conditions: 25.0 mg catalyst, 50.0 mL 20.0 mg/L RhB aqueous solution, reaction temperature = 30 °C, one 500 W Xe lamp (light intensity = 600 mW/cm^2, $\lambda > 420$ nm).

lower charge combination probability [36,37]. It could be ascribed that BiOBr nanosheets with thinner thickness in BOB–5–2–12 were favorable for the efficient separation of photo-generated electron–hole pairs and the rapid transfer of electrons to the surface of crystal [24,38].

3.3. Photocatalytic performance

The photodegradation of RhB under visible-light irradiation ($\lambda > 420$ nm) was used as a probe to evaluate the performances of different photocatalysts. According to the dependence of photodegradation rate on light irradiation time (Fig. 7), the degradation of RhB in the absence of photocatalyst could be neglected. BOB–5–2–12 could achieve the complete decomposition of RhB within 50 min, presenting much higher activity than both BOB–5–2–12(G) and BOB–Ref samples. It could be attributed that the hierarchical flower-like morphology assembled with nanosheets in BOB–5–2–12 could obtain stronger visible-light absorbance than 2D nanosheet structure via improving light multi-reflections. Additionally, the flower-like morphology could provide more efficient transportation of reactants [39]. The lower recombination of photo-generated electrons and holes also facilitated the promotion of photoactivity.

The linear relationship between $\ln(C/C_0)$ and reaction time (t) demonstrated that the RhB oxidation reaction was first order with respect to RhB concentration. The RhB-photodegradation rate at the reaction time of 40 min and the corresponding rate constant (k) for different catalysts are summarized in Table 1. BOB–5–2–12 revealed higher photoactivity than other BOB–X–2–12 sample owing to the large S_{BET} and the strong visible-light absorbance via light multi-reflections. The gradual agglomeration of nanosheets with the increased concentration of ethylene glycol was unfavorable for both visible light and reactants entering into the space between nanosheets. Meanwhile, the enlarged crystal size with increased thickness of nanosheet in BOB–40–2–12 was not beneficial to the separation and transportation of photo-generated electrons and holes, resulting in the low quantum efficiency [24].

In order to determine the active species during the photocatalytic oxidation pathway of RhB degradation on BiOBr catalyst, the ESR spectra of DMPO–$^{\bullet}O_2^-$ and DMPO–$^{\bullet}$OH adducts on BOB–5–2–12 catalyst without RhB under various conditions were shown in Fig. 8. Comparing to no obvious signals detected

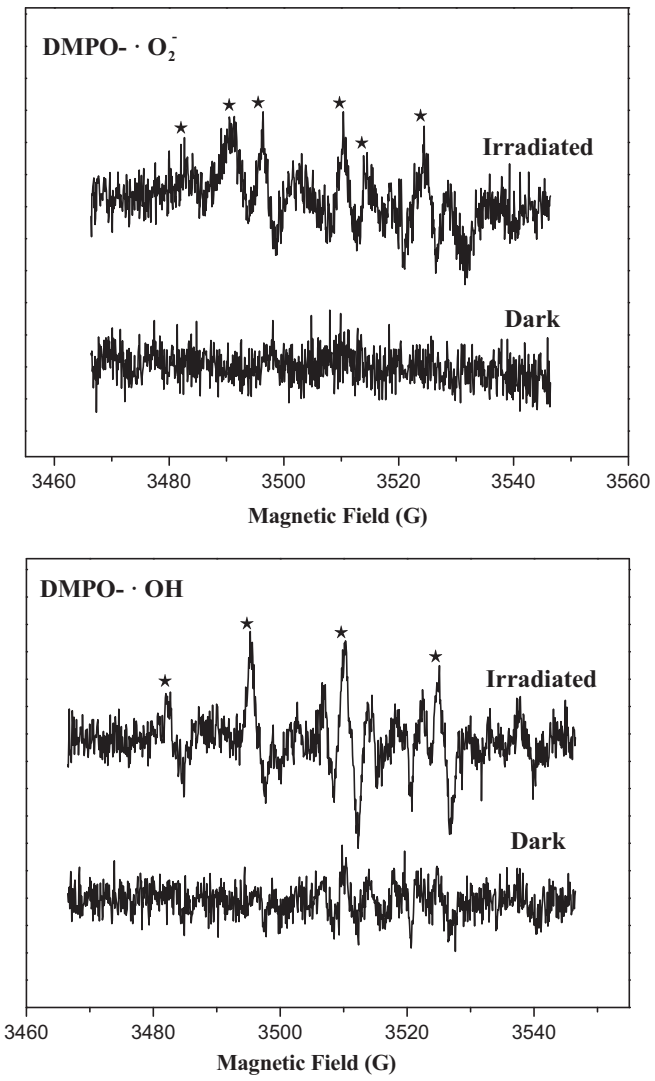

Fig. 8. ESR spectra of DMPO–$^{\bullet}O_2^-$ (top) and DMPO–$^{\bullet}$OH (bottom) adducts on BOB–5–2–12 catalyst without RhB under visible light irradiation ($\lambda > 420$ nm) and in dark, respectively.

in the dark, six characteristic peaks of DMPO–$^{\bullet}O_2^-$ and four of DMPO–$^{\bullet}$OH were observed under visible light irradiation. It demonstrated that BiOBr catalyst could be efficiently excited by visible light to create photo-generated electrons and holes, additionally, the time of charge separation was long enough to react with adsorbed oxygen/H_2O to produce $^{\bullet}O_2^-$ and $^{\bullet}$OH on the surface of BiOBr catalyst [40,41].

Furthermore, additional examination for the investigation of main active species during the photodegradation process was carried out via dissolving different trapping agents in the reaction solution before light irradiations. As shown in Fig. 9, the RhB degradation was significantly suppressed after trapping $^{\bullet}O_2^-$ by adding BQ. Trapping photo-generated holes and electrons with EDTA and $AgNO_3$, respectively, exhibited much weaker restraining effect to the photodegradation rate. However, TBA acted as $^{\bullet}$OH trapping agent presented no influence on photoactivity. It could be discovered that the $^{\bullet}O_2^-$ radical was the main active species during the photodegradation process. Therefore, the plausible reaction process could be proposed as follows. Under visible-light irradiations, holes were generated in valence band and electrons were transferred into conduct band in BiOBr crystal (Eq. (1)). The photo-generated electrons could reduce O_2 to form $^{\bullet}O_2^-$ and further

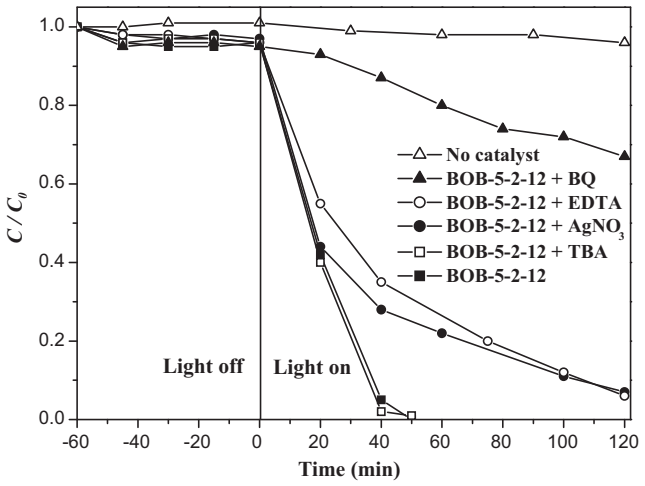

Fig. 9. Reaction process for photocatalytic degradation of RhB on BOB–5–2–12 catalyst with and without trapping agents. Reaction conditions were given in Fig. 7.

generate $^{\bullet}HO_2$ (Eqs. (2) and (3)). The change of pH value from 6.90 before reaction to 7.13 after reaction confirmed the formation of OH^- during the reaction. Then, $^{\bullet}O_2^-$ and $^{\bullet}HO_2$ could oxide the RhB molecular and holes could initiate the direct oxidation of RhB simultaneously (Eq. (4)).

$$BiOBr + h\nu(\geq Eg) \rightarrow h_{VB}^{+} + e_{CB}^{-} \quad (1)$$

$$e^- + O_2 \rightarrow {}^{\bullet}O_2^- \quad (2)$$

$$^{\bullet}O_2^- + H_2O \rightarrow {}^{\bullet}HO_2 + OH^- \quad (3)$$

$$h^+, {}^{\bullet}O_2^- \text{or} {}^{\bullet}HO_2 + RhB \rightarrow \text{degradedproduct} \quad (4)$$

Besides the high photoactivity, BiOBr catalyst also exhibited excellent durability during the photocatalytic reaction, which was very important for the practical application. According to Fig. 10, BOB–5–2–12 catalyst showed the stable activity after being reused for 6 times in the reaction system. The crystallization and hierarchical flower-like morphology were well maintained after recycling test, comparing to that of BOB–5–2–12 before reaction (see XRD patterns and FESEM image in Fig. S12). Furthermore, little Bi element in the solution could be measured after recycling reaction according to the ICP result. The excellent durability could be attributed that the high BiOBr crystallization could inhibit the decomposition of catalyst and the microsphere morphology could

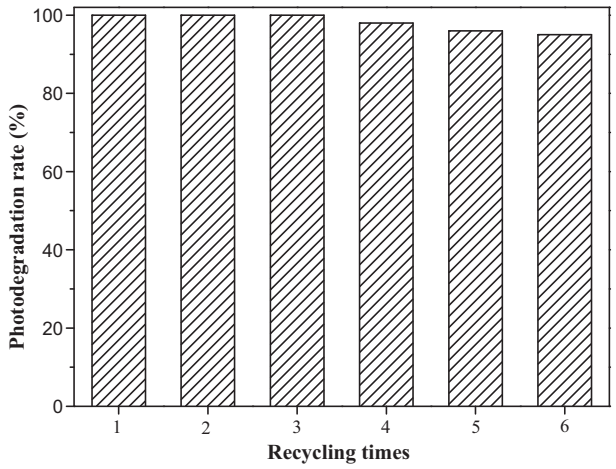

Fig. 10. Recycling test of BOB–5–2–12 catalyst. Reaction conditions: 25.0 mg catalyst, 50.0 mL 20.0 mg/L RhB aqueous solution, reaction time = 50 min, reaction temperature = 30 °C, one 500 W Xe lamp (light intensity = 600 mW/cm^2, λ > 420 nm).

prevent the agglomeration of nanosheets and achieve the easy solid/liquid separation. Additionally, the contrast test with other catalyst, such as CdS visible-light photocatalyst, which was prepared via the similar solvothermal process, demonstrated that both photoactivity and durability of BiOBr were much higher than those of CdS catalyst. After the photodegradation reaction for 2 h, the photodegradation rate of RhB on CdS was only 64%. Meanwhile, the activity of CdS catalyst was decreased sharply to only 5% after the recycling tests for 3 times, owing to the serious decomposition of CdS (about 90 wt.%). The high photoactivity and durability of BiOBr visible-light catalyst would show the great potential in practical application in the future.

4. Conclusion

This work developed a facile approach to prepare the hierarchical flower-like BiOBr microspheres via solvothermal method with both two-component solvent and surfactant. The growth of BiOBr crystal was influenced by the concentration of ethylene glycol and isopropanol in two-component solvent, the amount of CTAB surfactant and the solvothermal time. The high photocatalytic activity for RhB degradation under visible-light irradiations could be ascribed to the strong light absorbance with the light multi-reflection, the efficient separation of photo-generated electron–hole pairs, the high crystallization and the large surface area. The $^{\bullet}O_2^-$ radical was determined as main active species during the photodegradation process. Furthermore, the excellent durability of BiOBr catalyst was owing to the stable crystal phase and microsphere morphology, which was favorable for the potential practical applications.

Acknowledgments

This work was supported by National Natural Science Foundation of China (20937003), Shanghai Government (10230711600), State Key Laboratory of High Performance Ceramics and Superfine Microstructures (SKL200909SIC) and Shanghai Normal University (DZL807).

Appendix A. Supplementary data

Supplementary data associated with this article can be found, in the online version, at doi:10.1016/j.apcatb.2011.10.016.

References

[1] Z.G. Zou, J. Ye, K. Sayama, H. Arakawa, Nature 414 (2001) 625.
[2] X.B. Chen, S.S. Mao, Chem. Rev. 107 (2007) 2891.
[3] H.J. Zhang, G.H. Chen, D.W. Bahnemann, J. Mater. Chem. 19 (2009) 5089.
[4] J.C. Yu, J. Yu, W.K. Ho, Z.T. Jiang, L.Z. Zhang, Chem. Mater. 14 (2002) 3808.
[5] R. Asahi, T. Morikawa, T. Ohwaki, K. Aoki, Y. Taga, Science 293 (2001) 269.
[6] J.C. Yu, L. Wu, J. Lin, P. Li, Q. Li, Chem. Commun. (2003) 1552.
[7] Y.N. Huo, X.Y. Zhang, Y. Jin, J. Zhu, H.X. Li, Appl. Catal. B 83 (2008) 78.
[8] T. Kako, Z.G. Zou, M. Katagiri, J.H. Ye, Chem. Mater. 19 (2007) 198.
[9] Z.F. Bian, Y.N. Huo, Y. Zhang, J. Zhu, Y.F. Lu, H.X. Li, Appl. Catal. B 91 (2009) 247.
[10] Y.N. Huo, M. Miao, Y. Zhang, J. Zhu, H.X. Li, Chem. Commun. 47 (2011) 2089.
[11] Z.H. Ai, W.K. Ho, S.C. Lee, L.Z. Zhang, Environ. Sci. Technol. 43 (2009) 4143.
[12] S.Y. Chai, Y.J. Kima, M.H. Jung, A.K. Chakraborty, D. Jung, W.I. Lee, J. Catal. 262 (2009) 144.
[13] S.M. Sun, W.Z. Wang, L. Zhang, L. Zhou, W.Z. Yin, M. Shang, Environ. Sci. Technol. 43 (2009) 2005.
[14] J. Lee, Q. Zhang, F. Saito, J. Solid State Chem. 160 (2001) 469.
[15] N. Kijima, K. Matano, M. Saito, T. Oikawa, T. Konishi, H. Yasuda, T. Sato, Y. Yoshimura, Appl. Catal. A 206 (2001) 237.
[16] W.D. Wang, F.Q. Huang, X.P. Lin, Scr. Mater. 56 (2007) 669.
[17] J. Zhang, C.C. Tang, Chem. Mater. 20 (2008) 2937.
[18] W. Wang, F. Huang, X. Lin, J. Yang, Catal. Commun. 9 (2008) 8.
[19] Z. Jiang, F. Yang, G.D. Yang, L. Kong, M.O. Jones, T.C. Xiao, P.P. Edwards, J. Photochem. Photobiol. A 212 (2010) 8.
[20] J. Henle, P. Simon, A. Frenzel, S. Scholz, S. Kaskel, Chem. Mater. 19 (2007) 366.
[21] X. Zhang, Z.H. Ai, F.L. Jia, L.Z. Zhang, J. Phys. Chem. C 112 (2008) 747.
[22] B.B. Kale, J.O. Baeg, S.M. Lee, H. Chang, S.J. Moon, C.W. Lee, Adv. Funct. Mater. 16 (2006) 1349.

[23] Q. Zhao, Y. Xie, Z. Zhang, X. Bai, Cryst. Growth Des. 7 (2007) 153.
[24] M. Shang, W.Z. Wang, L. Zhang, J. Hazard. Mater. 167 (2009) 803.
[25] C. Minero, G. Mariella, V. Maurino, D. Vione, E. Pelizzetti, Langmuir 16 (2000) 8964.
[26] C.S. Pan, Y.F. Zhu, Environ. Sci. Technol. 44 (2010) 5570.
[27] M.C. Yin, Z.S. Li, J.H. Kou, Z.G. Zou, Environ. Sci. Technol. 43 (2009) 8361.
[28] Z.F. Bian, J. Zhu, S.H. Wang, Y. Cao, X.F. Qian, H.X. Li, J. Phys. Chem. C 112 (2008) 6258.
[29] M.W. Chu, M. Ganne, M.T. Caldes, L. Brohan, J. Appl. Phys. 91 (2002) 3178.
[30] P. Wang, B.B. Huang, Q.Q. Zhang, X.Y. Zhang, X.Y. Qin, Y. Dai, J. Zhan, J.X. Yu, H.X. Liu, Z.Z. Lou, Chem. Eur. J. 16 (2010) 10042.
[31] A.M. Cao, J.S. Hu, H.P. Liang, L.J. Wan, Angew. Chem. Int. Ed. 44 (2005) 4391.
[32] M.B. Gonzalez, A. Wu, P.M. Vilarinho, Chem. Mater. 18 (2006) 1737.
[33] J.H. Pan, H.Q. Dou, Z.G. Xiong, C. Xu, J.Z. Ma, X.S. Zhao, J. Mater. Chem. 20 (2010) 4512.
[34] M. Yoon, M. Seo, C. Jeong, J.H. Jang, K.S. Jeon, Chem. Mater. 17 (2005) 6069.
[35] H.X. Li, Z.F. Bian, J. Zhu, D.Q. Zhang, G.S. Li, Y.N. Huo, H. Li, Y.F. Lu, J. Am. Chem. Soc. 129 (2007) 8406.
[36] L.Q. Jing, Y.C. Qu, B.Q. Wang, S.D. Li, B.J. Jiang, L.B. Yang, W. Fu, H.G. Fu, J.Z. Sun, Sol. Energy Mater. Sol. Cells 90 (2006) 1773.
[37] H.M. Zhu, B.F. Yang, J. Xu, Z.P. Fu, M.W. Wen, T. Guo, S.Q. Fu, J. Zuo, S.Y. Zhang, Appl. Catal. B 90 (2009) 463.
[38] J. Hu, Y. Zhang, B. Liu, J. Liu, H. Zhou, Y. Xu, Y. Jiang, Z. Yang, Z.Q. Tian, J. Am. Chem. Soc. 126 (2004) 9470.
[39] L.Z. Zhang, J.C. Yu, Chem. Commun. 16 (2003) 2078.
[40] C. Hu, Y.Q. Lan, J.H. Qu, X.X. Hu, A.M. Wang, J. Phys. Chem. B 110 (2006) 4066.
[41] C.C. Chen, Q. Wang, P.X. Lei, W.J. Song, W.H. Ma, J.C. Zhao, Environ. Sci. Technol. 40 (2006) 3965.